OPTICS

There are many ways to spin a photon: Half-quantization of a total optical angular momentum

10.1126/sciadv.1501748

Kyle E. Ballantine,* John F. Donegan, Paul R. Eastham†

The angular momentum of light plays an important role in many areas, from optical trapping to quantum information. In the usual three-dimensional setting, the angular momentum quantum numbers of the photon are integers, in units of the Planck constant ħ. We show that, in reduced dimensions, photons can have a half-integer total angular momentum. We identify a new form of total angular momentum, carried by beams of light, comprising an unequal mixture of spin and orbital contributions. We demonstrate the half-integer quantization of this total angular momentum using noise measurements. We conclude that for light, as is known for electrons, reduced dimensionality allows new forms of quantization.

INTRODUCTION

Effects due to the angular momentum of light have been studied since the first measurements of the torques exerted on wave plates (*1*). Versions of these optomechanical effects now appear in experiments on optical trapping and manipulation (*2*) and enable the remote detection of rotation (*3*). Angular momentum effects are also emerging in the radio-frequency domain, for applications in astronomy and communications (*4*). Fundamental interest focuses on optical angular momentum in the quantum regime (*5*). The angular momentum of single photons has been measured (*6*), and entanglement (*7*) and Einstein, Podolsky and Rosen correlations (*8*) have been studied. This unique degree of freedom provides a basis for quantum information applications, with high-dimensional entanglement (*9*), quantum dense coding (*10*), and efficient object identification (*11*) recently demonstrated.

Central to these developments is the quantization of the angular momenta of the photon, which forms a discrete state space (*12*). The relevant quantum numbers are the eigenvalues of the spin and orbital angular momentum operators, S_z and L_z, in units of the reduced Planck constant ħ. The spin quantum number describes the circular polarization of light and takes values of ±1. The orbital quantum number appears in twisted beams, with phase-winding factors $e^{il\theta}$, where θ is the azimuthal angle, and takes integer values l (*13*). Thus, the quantum numbers for the total angular momentum, $J_z = L_z + S_z$, are the integers.

However, a general feature of two-dimensional systems is that angular momentum need not be quantized in the usual way. The orbital angular momentum of an electron orbiting in two dimensions around a magnetic flux need not be an integer, but can include an arbitrary fractional offset (*14*). The same mechanism introduces a phase factor in the exchange of particle-flux composites, implying that such particles have generalized or fractional statistics (*15*) as well as fractional spin. These concepts have played an important role in understanding the quantum Hall effect, where the low-lying quasiparticles have fractional statistics that are related to their fractional charge (*16*).

Here we show, in analogy to the theory of fractional spin particles (*14*), that an unexpected half-integer total angular momentum can arise for light. To do this, we note that the form $J_z = L_z + S_z$ for the total angular momentum of light follows from the rotational symmetry of Maxwell's equations (*17*, *18*). However, experiments involve beams of light propagating in a particular direction; thus, this full rotational symmetry is not present. The only potential symmetries, which determine the form of the angular momentum operators according to Noether's theorem, are rotations of the two-dimensional cross section of the beam around the propagation direction. We will show that this restricted symmetry leads to a new form of total angular momentum, which has a half-integer, that is, fermionic, spectrum. We will experimentally demonstrate this quantization by showing that the noise in the total angular momentum current corresponds to the fractional quantum ħ/2.

RESULTS

Forms of total angular momentum

We begin by establishing the possible forms of total angular momentum operator for photons in a beam of light. We consider the case of a paraxial beam, which is well approximated in experiments, and where the separation of spin and orbital angular momenta is well established (*19*). Such a beam is specified by a two-component complex vector field **E** (Jones vector), whose components give the amplitudes of each polarization across the beam. We take circularly polarized states as the basis and use polar coordinates (r,θ) across the beam. The angular momentum operators are the generators of rotations that act on this field. In the paraxial limit, they include the third Pauli matrix $S_z = \hbar\sigma_3$, which rotates the polarization direction homogeneously across the beam, and the usual orbital form $L_z = -i\hbar(d/d\theta)$, which rotates the beam profile (image) but leaves polarization unchanged (*20*). The eigenstates of S_z correspond to uniform, circularly polarized beams, and those of L_z correspond to uniformly polarized beams, such as Gauss-Laguerre beams, where the amplitude varies as $e^{il\theta}$.

For a general three-dimensional field, S_z and L_z are not valid as independent angular momenta because they do not preserve the transversality of the electromagnetic field (*17*, *21*). They appear in the usual combination $J_z = L_z + S_z$ for the total angular momentum, which is uniquely determined by the rotational invariance of Maxwell's equations in three space dimensions (*18*, *21*). However, in a beam of light, both polarization and image rotations, around the beam axis, keep the fields transverse, such that both spin and orbital angular momenta are valid

School of Physics and CRANN, Trinity College Dublin, Dublin 2, Ireland.
*Present address: Scottish Universities Physics Alliance, School of Physics and Astronomy, University of St Andrews, St Andrews KY16 9SS, UK.
†Corresponding author. Email: easthamp@tcd.ie

and independent (*13*, *22*). Thus, we may consider the possibility of a total angular momentum that is a general linear combination, $J_{z,\gamma} = L_z + \gamma S_z$.

The operator $J_{z,\gamma}$ generates simultaneous rotations of the polarization and image, in general, through different angles. As discussed below, it is related to measurements using devices that couple the spin and orbital degrees of freedom and can be defined for arbitrary γ. However, it corresponds to an angular momentum of the photon only if the field can be expanded in terms of its eigenfunctions. Thus, we seek those eigenfunctions, that is, the beams that are invariant, up to a phase factor, under the associated rotation. The solutions of the eigenvalue equation

$$(L + \gamma S)\mathbf{E} = j_\gamma \mathbf{E} \tag{1}$$

are of the form

$$\mathbf{E} = a_1 e^{il_1\theta}\mathbf{e}_R + a_2 e^{il_2\theta}\mathbf{e}_L \tag{2}$$

where $\mathbf{e}_{R/L}$ are right and left circularly polarized basis vectors, and the irrelevant radial dependence of the eigenmode is omitted. These modes are superpositions of two states with definite spin and orbital angular momenta. The quantum number, j_γ, of the conserved total angular momentum is given by

$$\gamma = (l_2 - l_1)/2$$
$$j_\gamma = (l_2 + l_1)/2$$

Equation 1 holds for any values of l_1 and l_2. However, the field should be unchanged by a complete rotation, implying that l_1 and l_2 must be integers. Beams with fractional l have been considered, but are not angular momentum eigenstates because they contain discontinuities that destroy rotational symmetry (*23*, *24*). On demanding integer l, we find that γ and j_γ are either both integers or both half-integers. Thus, we find two families of angular momentum operators. One family includes the existing forms L, S, and $L + S$, among others, where we now drop the z subscript. These have the expected bosonic spectrum with integer eigenvalues. The other family, typified by $L + S/2$, however, has a fermionic spectrum, comprising half-integer eigenvalues.

This half-integer total angular momentum is a quantized property of the photon. To see this, we note that the quantum theory is constructed by expanding the field in a complete set of transverse modes, with circularly polarized Laguerre-Gauss modes being the natural choice in the context of optical angular momentum (*25*). The eigenfunctions of J_γ, however, lead to other representations. For each γ, we find that there is an associated second-quantized angular momentum operator, which is the sum over modes of the number of photons in each, multiplied by the eigenvalue

$$\hat{J}_\gamma = \hat{L} + \gamma\hat{S} = \sum j_\gamma \hat{a}_\lambda^\dagger \hat{a}_\lambda$$

The mechanism behind this unexpected spectrum is analogous to that of an electron orbiting a fractional quantum of magnetic flux. For the electron, there is a fractional offset in the spectrum arising from the Aharonov-Bohm phase accumulated over a complete orbit around the flux line (*14*). For photons, a similar offset can be generated by choosing a non–uniformly polarized basis. The Berry phase (*26*) associated with the variation of polarization around a closed orbit then provides a synthetic gauge field, which shifts the angular momentum spectrum.

Measurement of generalized total angular momentum

These new forms of total angular momentum differ from the standard one, but nonetheless have the physical properties we expect. The established method for measuring an optical angular momentum, be it L, S, or $J_1 = L + S$, involves rotating the beams traversing a Mach-Zehnder interferometer (*6*). This measurement exploits the fact that eigenstates pick up a phase factor $e^{ij\phi}$ when rotated, where j is the quantum number of the measured angular momentum and ϕ is the rotation angle. We can generalize this technique to measure $J_{1/2}$, as shown in Fig. 1, by choosing wave plates and prisms, such that the image rotates by twice as much as the polarization, that is, by implementing the rotation corresponding to $J_{1/2}$.

We argue that the operator $J_{1/2}$ is an angular momentum because it is a generator of rotations and because it can be measured by interferometric techniques analogous to those previously used (*6*). It also has the required mechanical effects, as we now show. As with spin and orbital angular momenta, the torque exerted on an object depends on how it couples to the field. A half–wave plate, for example, reverses the sign of the spin quantum number σ = ±1 but leaves orbital angular momentum unchanged, and hence experiences a torque $2\hbar\sigma$ per photon (*1*). The inversion of orbital angular momentum, which is achieved by an ideal polarization-preserving Dove prism, implies a torque $2\hbar l$ per photon (*27*). For the total angular momentum J_γ, the quantum number is reversed on transmission through a polarization-preserving Dove prism followed by two half–wave plates, one with a constant fast axis and the other with a fast axis at an angle γθ where the azimuthal angle is θ [that is, a q plate (*28*) with charge $q = \gamma$]. We calculate that the torque exerted on such an element by a beam with quantum number j_γ is $2\hbar j_\gamma$ per photon. Thus,

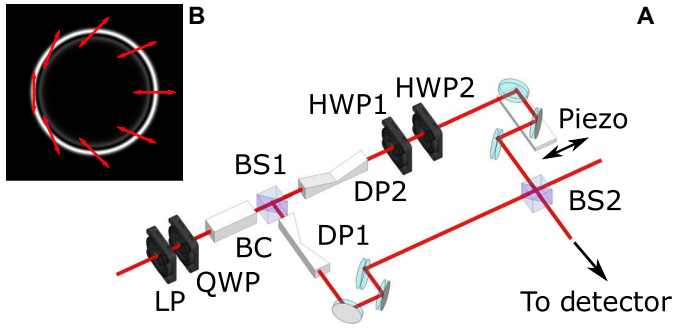

Fig. 1. The generalized total angular momentum of light. (**A**) Experimental arrangement to study the generalized total angular momentum of light $J_{1/2}$. Photons in a variable superposition of two angular momentum eigenstates $|j = \pm 1/2\rangle$ can be generated from the Gaussian input beam using a linear polarizer (LP), a quarter–wave plate (QWP), and a biaxial crystal (BC). The angular momentum currents can then be measured using an interferometer, introducing rotations in the optical paths to sort the beam according to angular momentum. Measuring $J_{1/2}$ entails rotating the image and polarization by different angles, in this case using two polarization-preserving Dove prisms (DP1 and DP2) to rotate the image by 180° and two half–wave plates (HWP1 and HWP2) to rotate the polarization by 90°. BS1 and BS2 are beam splitters used to separate and recombine the optical paths; DP1 and DP2 are at 90° to one another, and HWP1 and HWP2 are at 45°. The piezo delay is tuned such that each eigenstate interferes constructively at one output and destructively at the other. (**B**) Calculated intensity (grayscale) and polarization (red arrows) for the $|j = 1/2\rangle$ component of the input beam.

the change in the eigenvalue of J_γ is related to a torque as it should be, confirming on mechanical grounds that it represents a form of angular momentum. Because $j_{1/2}$ has a half-integer spectrum, the minimum torque exerted when this quantum number reverses is $\hbar$, whereas for the standard quantum numbers l, σ, and j, the corresponding value is $2\hbar$.

We have used this interferometer to measure the angular momentum $J_{1/2}$ of photons in beams formed from two of its eigenstates, $|j_{1/2} = \pm 1/2\rangle$. These beams are generated by the conical refraction (*29*) of the light from a helium-neon laser. As shown in Fig. 1, the light is first elliptically polarized before passing through a biaxial crystal, leading to a superposition of angular momentum eigenstates. The amplitudes in the superposition are controlled by the angle of the QWP, θ_{qwp}, with the beam varying from purely $|j_{1/2} = 1/2\rangle$ to purely $|j_{1/2} = -1/2\rangle$ as the QWP rotates by 90°. This beam then enters a Mach-Zehnder interferometer, where two polarization-preserving Dove prisms at 90° and two half–wave plates at 45° rotate the beam to impart a relative phase of π between the components $|j_{1/2} = \pm 1/2\rangle$. The path lengths are tuned such that each component interferes constructively at one output port and destructively at the other, and the signal is detected with a photodiode. The angular momentum current is thus related to the rates of photon arrivals P_1, P_2 at the two outputs and the corresponding photocurrents I_1, I_2 by

$$\langle \hat{M}_{1/2} \rangle = \frac{\hbar}{2}(P_1 - P_2) = \frac{\hbar}{2e}(I_1 - I_2) \tag{3}$$

[the quantum efficiency of the detector will be irrelevant for the following because we have Poissonian intensity statistics (*30*), and so is taken as one]. The average angular momentum per photon is obtained by dividing by the total flux or photocurrent. The result is shown in Fig. 2A and confirms that the average angular momentum per photon varies between $+\hbar/2$ and $-\hbar/2$.

Noise in angular momentum currents

To establish the quantization of angular momentum, we have studied its fluctuations, in particular the noise in the angular momentum current. Electrical current noise is known to reveal the discreteness of charge and has been used particularly to demonstrate the fractional charge of quasiparticles in quantum Hall states (*31*–*33*). This suggests that angular momentum current noise could, analogously, reveal the discreteness of optical angular momentum.

To establish the possibilities of such diagnostics, we first calculate the noise properties of the angular momentum currents. We consider measurements involving a finite response time T, such that the operator for the angular momentum current is $\hat{M}_\gamma(T) = \frac{1}{T}\int_t^{t+T} dt' \hat{J}_\gamma$, and use wave packet quantization to calculate the moments of $\hat{M}_\gamma$. For a single photon in an eigenstate of $J_{1/2}$, we obtain $\langle \hat{M}_{1/2} \rangle = \hbar j_{1/2}/T$, as expected; we also find that the variance of the current operator $\hat{M}_{1/2}$, $\sigma^2_{1/2} = \langle \hat{M}^2_{1/2} \rangle - \langle \hat{M}_{1/2} \rangle^2$, is zero. This is consistent with the assertion that each photon carries an exact amount of this total angular momentum. In contrast, for this state, we obtain a nonzero variance for the orbital and spin current operators, $\hat{M}_L$ and $\hat{M}_S$. Physically, a measurement of orbital or spin angular momentum projects onto the components of the superposition in Eq. 2, introducing quantum noise in these currents.

Alternatively, we can consider the angular momentum currents in the semiclassical limit, that is, for the coherent states originating from the laser in our experiment. In this limit, in general, quantization of current carriers appears as shot noise (*30*), with power spectral density

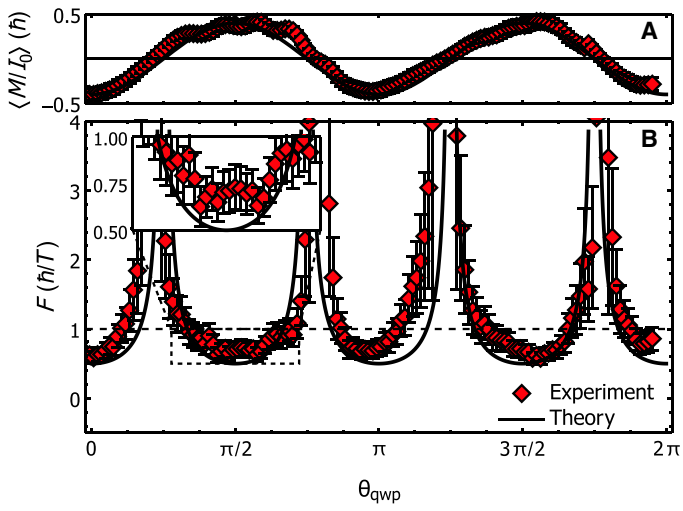

Fig. 2. Experimental results. (**A**) Average of the total angular momentum $J_{1/2}$ per photon, in beams comprising a variable superposition of its eigenstates $|j = 1/2\rangle$ and $|j = -1/2\rangle$. The solid line is the predicted result, corrected for the measured visibility of the interferometer. (**B**) Measured fluctuations in the angular momentum current quantified by its Fano factor. At the minima, the noise is predominantly shot noise reflecting the discreteness of angular momentum. The corresponding charge goes below $\hbar$ and approaches the expected value of $\hbar/2$, showing that the quantized angular momentum of the photon is a fraction of $\hbar$. The solid lines show the predicted result in the ideal case, with full visibility and no classical noise.

$2qI$, where q is the charge and I is the current. The discrete charge q can thus be obtained from the Fano factor, that is, the ratio between current noise and current. To elucidate this, we calculate the mean and variance of the angular momentum currents for coherent states. For a spatial mode that is an eigenstate of J_γ, we find

$$\langle \hat{M}_\gamma \rangle = \frac{\hbar}{T} j_\gamma$$
$$\sigma^2_\gamma = \frac{\hbar j_\gamma}{T} \langle \hat{M}_\gamma \rangle$$

which is the expected result for shot noise with quantized charge $\hbar j_\gamma$. To calculate the noise for a general beam, we note that any beam is a superposition of Laguerre-Gauss modes with amplitudes $c_{l,\sigma}$ and write $\hat{a} = \sum_{l,\sigma} c_{l,\sigma} \hat{a}_{l,\sigma}$. In this way, we find that the Fano factor in a general coherent state is

$$F_\gamma = \frac{\sigma^2_\gamma}{|\langle \hat{M}_\gamma \rangle|} = \frac{\hbar \Sigma (l + \gamma\sigma)^2 |c_{l,\sigma}|^2}{T |\Sigma (l + \gamma\sigma) |c_{l,\sigma}|^2|} \geq \frac{\hbar}{2T} \tag{4}$$

Thus, the minimum noise of an angular momentum current in the semiclassical limit corresponds to the quantum $\hbar/2$ and is achieved in measurements of $J_{1/2}$ on beams that are eigenstates thereof. This noise is solely the shot noise associated with the discreteness of angular momentum. Note that for any angular momentum operator, Eq. 4 implies that the minimum noise is achieved in the corresponding eigenstate, specifically that with the lowest-magnitude nonzero eigenvalue. This shot noise limit is, thus, minimized for

operators with half-integer spectra. Moreover, we see that for beams that are not eigenstates, the noise is larger, as a result of the uncertainty in the angular momentum of each photon.

Experimental demonstration of half-quantization

To experimentally demonstrate the half-integer quantization, we have measured the Fano factor $F_{1/2}$ for the same input beams discussed above. We amplify and digitize the photocurrent at one output of our interferometer, and extract the noise power at 3 MHz. This allows us to compute the noise power in the angular momentum current: From Eq. 3, we find

$$\sigma^2_{1/2} = \frac{\hbar^2}{4}\left(\sigma^2_{P_1} + \sigma^2_{P_2}\right) = \frac{\hbar^2}{4e^2}\left(\sigma^2_{I_1} + \sigma^2_{I_2}\right) \quad (5)$$

using the fact that our input beams are, to a good approximation, coherent states, such that photodetections at each output are independent. We measure the photocurrent and noise at one port as a function of θ_{qwp}, which allows us to deduce the corresponding quantities for the other port by symmetry, because increasing θ_{qwp} by 90° is equivalent to exchanging the two outputs. In practice, vibrations and drift of the interferometer during the rotation of the QWP cause slight differences between these quantities, which are accounted for in our error estimates.

The Fano factor, divided by $1/T = 2\Delta f$, where Δf is the frequency resolution, is plotted in Fig. 2B, again as the beam varies between $|j_{1/2} = 1/2\rangle$ and $|j_{1/2} = -1/2\rangle$. The noise is minimized when the beam is in one of these two eigenstates and is bounded from below by $\hbar/2$. The Fano factor, in units of $\hbar/T$, clearly goes below one and approaches the limit of one-half at each minima, as predicted by Eq. 4. This demonstrates that each photon carries a total angular momentum $J_{1/2}$ that is a fraction of $\hbar$. Note that the ideal theoretical value of $\hbar/2$ is a lower bound on the result; contributions from classical noise and limitations on the visibility of the interferometer mean that this lower bound is not necessarily achieved.

DISCUSSION

Here, we have considered beams close to the paraxial limit and have shown how the independence of spin and orbital angular momenta allows for a new definition of total angular momentum. However, it has recently been shown that independent spin and orbital angular momenta can be defined beyond this limit (*19*, *34*, *35*). This immediately provides the nonparaxial generalization of the total angular momentum component J_γ, on replacing the paraxial forms for spin and orbital angular momenta, assumed here, with the nonparaxial ones. The nonparaxial spin and orbital angular momenta are independently conserved; hence, this would be a conserved quantity as well. They are modified forms of the rotation operators, specifically the transverse parts of those that rotate the field vectors (spin) and image (orbital) around the specified axis. The corresponding total angular momentum J_γ generates these modified rotations simultaneously, in a fixed ratio γ.

The new form of total angular momentum we have identified gives an alternative representation of the state space in terms of beams with nonuniform polarization, leading to a new understanding of the effects of optical angular momentum. Its half-integer spectrum shows that for light, as is already known for electronic systems, reduced dimensionality allows for new forms of quantization. The half-integer quantization, which we demonstrate through noise measurements, implies fermionic exchange statistics, and an important extension of our work will be to identify the measurable consequences of such photonic fermionization.

MATERIALS AND METHODS

Theory of the interferometer

We show how the interferometer shown in Fig. 1 can be used to measure the quantum statistics of the angular momentum $J_{1/2}$, as quantified by the moments of its current distribution. Operationally, it is a Mach-Zehnder interferometer in which the beam is rotated by angle ϕ_0 in one arm, whereas a phase shift δ is introduced in the other. The beam splitter formalism gives the field operators at the two output ports to be

$$\hat{a}_1 = \frac{i}{2}\left(e^{i\delta} + U\right)\hat{a}$$

$$\hat{a}_2 = \tfrac{1}{2}\left(e^{i\delta} - U\right)\hat{a}$$

where $\hat{a}$ is the input field. We omit the operators for the second input port, which act on the vacuum, because they would not contribute to the expectation values of normal-ordered operators considered here. The operator U acts on the spatial and spin coordinates to rotate the field, and for the rotation generated by the angular momentum operator, J_γ is $e^{i\phi_0 J_\gamma}$. In the eigenbasis of orbital and spin angular momenta, the operators have indices l and $\sigma = \pm 1$ acted on by the angular momentum operators as $L_z\hat{a}_{l,\sigma} = l\hat{a}_{l,\sigma}$ and $J_\gamma\hat{a}_{l,\sigma} = (l + \gamma\sigma)\hat{a}_{l,\sigma}$.

We were concerned with the case where $\gamma = 1/2$ and with the subspace where $j = \pm 1/2$. This subspace involves operators $\hat{a}_{0,1}$, $\hat{a}_{1,-1}$ with $j = 1/2$ and $\hat{a}_{-1,1}$, $\hat{a}_{0,-1}$ with $j = -1/2$. Choosing $\delta = \pi/2$ and $\phi_0 = \pi$ gives $\hat{a}_1 = -\hat{a}_{l,\sigma}$, $\hat{a}_2 = 0$ for the first class and $\hat{a}_1 = 0$, $\hat{a}_2 = i\hat{a}_{l,\sigma}$ for the second class, showing that the interferometer will sort the beam according to the eigenvalue of $J_{1/2}$. Because any linear combination of fields with $j = 1/2$ will be transmitted to the first port and any combination with $j = -1/2$ will be transmitted to the second port, we have

$$\begin{aligned}\hat{M} &= \sum_{l,\sigma}(l + \sigma/2)\hat{a}^\dagger_{l,\sigma}\hat{a}_{l,\sigma} \\ &= \frac{1}{2}\hat{a}^\dagger_{0,1}\hat{a}_{0,1} + \frac{1}{2}\hat{a}^\dagger_{1,-1}\hat{a}_{1,-1} - \frac{1}{2}\hat{a}^\dagger_{0,-1}\hat{a}_{0,-1} - \frac{1}{2}\hat{a}^\dagger_{-1,1}\hat{a}_{-1,1} \\ &= \frac{1}{2}\left(\hat{a}^\dagger_1\hat{a}_1 - \hat{a}^\dagger_2\hat{a}_2\right)\end{aligned}$$

when the angular momentum current operator is restricted to the subspace in question. Because this combination of the output intensity operators is the same as the angular momentum current operator, restricted to a particular subspace, its mean and higher moments will all be identical, provided the input beam is contained wholly in that subspace. This result generalizes in the expected manner to higher-dimensional subspaces, where the beam could be sorted using a cascade of interferometers (*6*).

Details of the input beams

The structured beams analyzed by our interferometer were generated by a combination of polarization optics (the LP and the QWP in

Fig. 1) and a BC, with the BC acting as a partial spin angular momentum–to–orbital angular momentum converter. The beam following the LP was a linearly polarized Gaussian, which was then incident on the QWP, with a fast axis at angle $\theta_{qwp} + \pi/4$ to the polarization (the offset simplifies the following results). This led to a variable superposition of right and left circularly polarized Gaussian beams, with amplitudes

$$\begin{aligned} A_R &= e^{i(\theta_{qwp}+\pi/4)}\cos(\theta_{qwp}) \\ A_L &= e^{-i(\theta_{qwp}+\pi/4)}\sin(\theta_{qwp}) \end{aligned} \tag{6}$$

These two circularly polarized components, with $l = 0$ and helicity $\sigma = \pm 1$, underwent conical refraction in the BC to become (*29*)

$$|l,\sigma\rangle = |0,1\rangle \rightarrow \frac{1}{\sqrt{2}}(|1,-1\rangle + |0,1\rangle) \equiv |j = 1/2\rangle$$

$$|0,-1\rangle \rightarrow \frac{1}{\sqrt{2}}(|-1,1\rangle + |0,-1\rangle) \equiv |j = -1/2\rangle$$

that is, eigenstates of the mixed angular momentum $J_{1/2}$ with eigenvalues $\pm 1/2$, as indicated. The polarization and intensity profile (*29*) of one of these components, in the focal image plane of the BC, are shown in Fig. 1B. The orbital angular momentum and polarization of a conically refracted beam are well understood and have been measured previously (*36*). Thus, the generated beam was a superposition of $|j = \pm 1/2\rangle$, with amplitudes given by Eq. 6 as functions of the QWP angle.

Experimental details

As shown in Fig. 1, light from a helium-neon laser was passed through a Glan-Thompson polarizer and a wavelength-specific QWP to create a combination of circular polarizations. This combination was passed through a BC and a lens pair (not shown) to create a collimated conical beam, with the focal image plane at infinity, containing a superposition of the modes $|j = \pm 1/2\rangle$. This input beam was then incident on a 50:50 nonpolarizing beam splitter that separated it into the two arms of a Mach-Zehnder interferometer. Within this interferometer, the two images were rotated relative to one another by 180° and the two polarization directions were rotated by 90°. The image rotation was achieved using a pair of Dove prisms, and the polarization rotation was achieved using a pair of half–wave plates. For space reasons, the image rotation was achieved with one prism in each arm of the interferometer. The prisms were not of the conventional form, because that would lead to an angle-dependent effect on the polarization, in addition to the desired transformation of the image. We instead used the previously described structure (*6*), which inverted the image and acted as a QWP. In our case, these effective QWPs did not affect the operation of the interferometer and did not need to be compensated for. The top arm had a pair of mirrors, acting as a delay line, on a piezo translation stage. This stage could be varied with a resolution ≈10 nm, leading to a resolution in the path length of ≈20 nm. There was a similar delay line element in the second arm, on a manual translation stage, allowing for roughly equal path lengths (this was necessary as the beam had some spatial evolution; the interferometer did not need to be at the zero-order fringe).

The two paths recombined at a second beam splitter, and the beams exited the interferometer from one of two output ports. The output of one port was focused onto a photodiode, which was used to measure both the intensity and its noise. The current from the photodiode was converted to a voltage using a low-noise transimpedance amplifier, and this voltage was sampled with an oscilloscope. The voltages for each port were, thus, related to the photocurrents by $V_{1,2} = GI_{1,2}$, with transimpedance $G = 2.55$ kilohm. Equations 3 and 5 allowed us to extract the Fano factor for the angular momentum from the voltages and their fluctuations

$$F_{1/2} = \frac{\hbar}{2eG}\frac{\sigma_{V_1}^2 + \sigma_{V_2}^2}{V_1 - V_2} = \frac{\hbar}{2eG}\frac{\sigma_{V_1}^2(\theta) + \sigma_{V_1}^2(\theta - \pi/2)}{2V_1 - V_0}$$

In the second equality, we used the fact that rotating the QWP by $\pi/2$ is equivalent to exchanging the ports, allowing only one to be measured, and also that $V_1 + V_2 = V_0$ is constant.

Error analysis

The dominant contribution to the error bars in Fig. 2B was the instability and vibration of the interferometer. Because the output of the second port at a given time was calculated as the output of the first port at a different time, these fluctuations meant that the sum of the voltages $V_1 + V_2$ departed from the constant V_0. We displayed this as an uncertainty in the measured Fano factor obtained from the uncertainty in V_0. The error in the measured noise gave a smaller contribution, because this was obtained as an average over 1000 periodograms, yielding a fractional error of the order $1/\sqrt{1000} \approx 3\%$.

For us to realize the shot noise limit for the angular momentum current, we had to use shot noise limited light. This behavior, as well as the calibration of G, was confirmed using the relation between the measured voltage noise and voltage (*37*). The noise

$$\sigma^2 = \sigma_0^2 + \alpha V + \beta V^2 + r \tag{7}$$

comprises a background contribution, shot noise that depends linearly on the signal, classical noise that depends quadratically on the signal, and a random error proportional to the true noise. The linear term has a coefficient

$$\alpha = 2e\Delta f G \tag{8}$$

Figure S1 shows the measured noise, along with a fit to Eq. 7 using Eq. 8 with the nominal $G = 2.55$ kilohm. The agreement confirms this value and, furthermore, that we were operating in the shot noise limited regime. The SD of the residuals is 90 V^2/A, consistent with the relative error on the noise estimated above.

Calculations of the current statistics

The calculations of the angular momentum statistics reported in Results concern the time-averaged current operator

$$\hat{M}_\gamma(t) = \frac{1}{T}\int_t^{t+T} dt' \sum_{\sigma,l} \hbar(l + \gamma\sigma)\hat{a}_{l,\sigma}^\dagger(t')\hat{a}_{l,\sigma}(t') \tag{9}$$

where T is the response time of the detector. This is equal to the angular momentum in each mode multiplied by the number current of photons in that mode, summed over all modes and averaged over the response time. A nonperfect efficiency is not included because it

would merely add some excess shot noise (*30*). The time dependence of the beam was encoded by using the wave packet states

$$\hat{a}_{\xi;l,\sigma} = \int dt\, \xi(t) \hat{a}_{l,\sigma}(t)$$

which can also be combined into superpositions of modes

$$\hat{a}_{\xi} = \sum_{l,\sigma} \alpha_{l,\sigma} \hat{a}_{\xi;l,\sigma}$$

The function $\xi(t)$ controls the time dependence of the photon number current but does not affect the angular momentum per photon. The states examined consist of single-photon states

$$|1\rangle = \hat{a}_{\xi}^{\dagger}|0\rangle \tag{10}$$

and coherent states

$$|c\rangle = \exp(\hat{a}_{\xi}^{\dagger} - \hat{a}_{\xi})|0\rangle \tag{11}$$

The expectation value of the angular momentum current operator and its higher powers can now be calculated. The operator in Eq. 9 or its higher powers can be placed between the states given by Eqs. 10 and 11. The commutation relations (*30*)

$$[\hat{a}_{l,\sigma}(t), \hat{a}_{l',\sigma'}^{\dagger}(t')] = \delta_{l,l'}\delta_{\sigma,\sigma'}\delta(t-t')$$
$$[\hat{a}_{l,\sigma}^{\dagger}(t), \hat{a}_{l',\sigma'}^{\dagger}(t')] = [\hat{a}_{l,\sigma}(t), \hat{a}_{l',\sigma'}(t')] = 0$$

were used to evaluate the angular momentum current expectation value or variance in terms of the time-dependent classical current, which is proportional to $\int dt|\xi(t)|^2$.

Torques due to a mixed angular momentum

In Results, we stated that the eigenvalue of J_γ was reversed by a polarization-preserving Dove prism followed by two half–wave plates, one with a constant fast axis and the other with a fast axis that makes an angle $\gamma\theta$ to the x axis when the polar angle is θ. To show this, we note that the effect of the Dove prism on the field is to send the polar angle $\theta \rightarrow -\theta$, whereas the half–wave plates have a combined Jones matrix, in the basis of circular polarizations

$$\begin{pmatrix} 0 & e^{-2i\gamma\theta} \\ e^{2i\gamma\theta} & 0 \end{pmatrix}\begin{pmatrix} 0 & 1 \\ 1 & 0 \end{pmatrix} = \begin{pmatrix} e^{-2i\gamma\theta} & 0 \\ 0 & e^{2i\gamma\theta} \end{pmatrix}$$

Thus, the effect on an eigenstate of the form given in Eq. 2 is

$$\begin{pmatrix} a_1 e^{il_1\theta} \\ a_2 e^{il_2\theta} \end{pmatrix} \overset{\text{DP}}{\rightarrow} \begin{pmatrix} a_1 e^{-il_1\theta} \\ a_2 e^{-il_2\theta} \end{pmatrix} \overset{\text{HWPs}}{\rightarrow} \begin{pmatrix} a_1 e^{-il_2\theta} \\ a_2 e^{-il_1\theta} \end{pmatrix} \equiv \begin{pmatrix} a_1 e^{il_1'\theta} \\ a_2 e^{il_2'\theta} \end{pmatrix}$$

where we have used $\gamma = (l_2 - l_1)/2$. The resulting field has $\gamma' = (l_2' - l_1')/2 = \gamma$, but the eigenvalue is reversed $j_\gamma' = (l_2' + l_1')/2 = -j_\gamma$. For the case where the device was rotated as a whole by angle α, we found the same output field, but with an additional phase factor $e^{2ij_\gamma\alpha}$.

The change in angular momentum of the beam implies a torque, which we calculated following the argument previously given for the orbital case (*27*). If the device was spinning with an angular velocity Ω, then $\alpha = \Omega t$ and the phase factor $e^{2ij_\gamma\alpha}$ becomes a rotational Doppler shift (*27*, *38*) by the angular frequency $2j_\gamma\Omega$. This implies a change in energy E of each photon crossing the device, exerting a torque $\tau = dE/d\Omega = 2\hbar j_\gamma$.

SUPPLEMENTARY MATERIALS

Supplementary material for this article is available at http://advances.sciencemag.org/cgi/content/full/2/4/e1501748/DC1

fig. S1. Calibration of the noise measurement.

REFERENCES AND NOTES

1. R. A. Beth, Mechanical detection and measurement of the angular momentum of light. *Phys. Rev.* **50**, 115–125 (1936).
2. M. Padgett, R. Bowman, Tweezers with a twist. *Nat. Photonics* **5**, 343–348 (2011).
3. M. P. J. Lavery, F. C. Speirits, S. M. Barnett, M. J. Padgett, Detection of a spinning object using light's orbital angular momentum. *Science* **341**, 537–540 (2013).
4. B. Thidé, H. Then, J. Sjöholm, K. Palmer, J. Bergman, T. D. Carozzi, Y. N. Istomin, N. H. Ibragimov, R. Khamitova, Utilization of photon orbital angular momentum in the low-frequency radio domain. *Phys. Rev. Lett.* **99**, 087701 (2007).
5. G. Molina-Terriza, J. P. Torres, L. Torner, Twisted photons. *Nat. Phys.* **3**, 305–310 (2007).
6. J. Leach, J. Courtial, K. Skeldon, S. M. Barnett, S. Franke-Arnold, M. J. Padgett, Interferometric methods to measure orbital and spin, or the total angular momentum of a single photon. *Phys. Rev. Lett.* **92**, 013601 (2004).
7. A. Mair, A. Vaziri, G. Weihs, A. Zeilinger, Entanglement of the orbital angular momentum states of photons. *Nature* **412**, 313–316 (2001).
8. J. Leach, B. Jack, J. Romero, A. K. Jha, A. M. Yao, S. Franke-Arnold, D. G. Ireland, R. W. Boyd, S. M. Barnett, M. J. Padgett, Quantum correlations in optical angle–orbital angular momentum variables. *Science* **329**, 662–665 (2010).
9. J. Romero, D. Giovannini, S. Franke-Arnold, S. M. Barnett, M. J. Padgett, Increasing the dimension in high-dimensional two-photon orbital angular momentum entanglement. *Phys. Rev. A* **86**, 012334 (2012).
10. J. T. Barreiro, T.-C. Wei, P. G. Kwiat, Beating the channel capacity limit for linear photonic superdense coding. *Nat. Phys.* **4**, 282–286 (2008).
11. N. Uribe-Patarroyo, A. Fraine, D. S. Simon, O. Minaeva, A. V. Sergienko, Object identification using correlated orbital angular momentum states. *Phys. Rev. Lett.* **110**, 043601 (2013).
12. N. K. Langford, R. B. Dalton, M. D. Harvey, J. L. O'Brien, G. J. Pryde, A. Gilchrist, S. D. Bartlett, A. G. White, Measuring entangled qutrits and their use for quantum bit commitment. *Phys. Rev. Lett.* **93**, 053601 (2004).
13. L. Allen, M. W. Beijersbergen, R. J. C. Spreeuw, J. P. Woerdman, Orbital angular momentum of light and the transformation of Laguerre-Gaussian laser modes. *Phys. Rev. A* **45**, 8185–8189 (1992).
14. F. Wilczek, Magnetic flux, angular momentum, and statistics. *Phys. Rev. Lett.* **48**, 1144–1146 (1982).
15. F. Wilczek, Quantum mechanics of fractional-spin particles. *Phys. Rev. Lett.* **49**, 957–959 (1982).
16. D. Arovas, J. R. Schrieffer, F. Wilczek, Fractional statistics and the quantum Hall effect. *Phys. Rev. Lett.* **53**, 722–723 (1984).
17. S. J. van Enk, G. Nienhuis, Spin and orbital angular momentum of photons. *Europhys. Lett.* **25**, 497–501 (1994).
18. L. Allen, S. Barnett, M. Padgett, Eds., *Optical Angular Momentum* (Institute of Physics, Bristol, UK, 2003).
19. K. Y. Bliokh, J. Dressel, F. Nori, Conservation of the spin and orbital angular momenta in electromagnetism. *New J. Phys.* **16**, 093037 (2014).
20. M. V. Berry, Paraxial beams of spinning light, in *Proc. SPIE 3487, International Conference on Singular Optics*, Partenit, Crimea, Ukraine, 5 October 1997 (SPIE, Bellingham, WA, 1998).
21. C. Cohen-Tannoudji, J. Dupont-Roc, G. Grynberg, *Photons and Atoms: Introduction to Quantum Electrodynamics* (Wiley, New York, 1997), 486 pp.
22. S. M. Barnett, Optical angular-momentum flux. *J. Opt. B Quantum Semiclassical Opt.* **4**, S7–S16 (2002).
23. M. V. Berry, Optical vortices evolving from helicoidal integer and fractional phase steps. *J. Opt. A Pure Appl. Opt.* **6**, 259–268 (2004).
24. J. B. Götte, S. Franke-Arnold, R. Zambrini, S. M. Barnett, Quantum formulation of fractional orbital angular momentum. *J. Mod. Opt.* **54**, 1723–1738 (2007).

25. G. F. Calvo, A. Picón, E. Bagan, Quantum field theory of photons with orbital angular momentum. *Phys. Rev. A* **73**, 013805 (2006).
26. M. V. Berry. Quantal phase factors accompanying adiabatic changes, *Proc. R. Soc. London Ser. A.* **392**, 45–57 (1984).
27. G. Nienhuis. Doppler effect induced by rotating lenses, *Opt. Commun.* **132**, 8–14 (1996).
28. L. Marrucci, C. Manzo, D. Paparo, Optical spin-to-orbital angular momentum conversion in inhomogeneous anisotropic media. *Phys. Rev. Lett.* **96**, 163905 (2006).
29. M. V. Berry, M. R. Jeffrey, M. Mansuripur, Orbital and spin angular momentum in conical diffraction. *J. Opt. A Pure Appl. Opt.* **7**, 685–690 (2005).
30. R. Loudon, *The Quantum Theory of Light* (Oxford Univ. Press, Oxford, 1983).
31. C. L. Kane, M. P. A. Fisher, Nonequilibrium noise and fractional charge in the quantum Hall effect. *Phys. Rev. Lett.* **72**, 724–727 (1994).
32. R. de-Picciotto, M. Reznikov, M. Heiblum, V. Umansky, G. Bunin, D. Mahalu, Direct observation of a fractional charge. *Nature* **389**, 162–164 (1997).
33. M. Dolev, M. Heiblum, V. Umansky, A. Stern, D. Mahalu, Observation of a quarter of an electron charge at the $\nu = 5/2$ quantum Hall state. *Nature* **452**, 829–834 (2008).
34. R. P. Cameron, F. C. Speirits, C. R. Gilson, L. Allen, S. M. Barnett, The azimuthal component of Poynting's vector and the angular momentum of light. *J. Opt.* **17**, 125610 (2015).
35. A. Aiello, M. V. Berry, Note on the helicity decomposition of spin and orbital optical currents. *J. Opt.* **17**, 062001 (2015).
36. D. P. O'Dwyer, C. F. Phelan, Y. P. Rakovich, P. R. Eastham, J. G. Lunney, J. F. Donegan, The creation and annihilation of optical vortices using cascade conical diffraction. *Opt. Express* **19**, 2580–2588 (2011).
37. H.-A. Bachor, T. C. Ralph, *A Guide to Experiments in Quantum Optics* (Wiley-VCH, Weinheim, Germany, 2004), 434 pp.
38. R. Simon, H. J. Kimble, E. C. G. Sudarshan, Evolving geometric phase and its dynamical manifestation as a frequency shift: An optical experiment. *Phys. Rev. Lett.* **61**, 19–22 (1988).

Acknowledgments: We thank M. Padgett, S. Barnett, and J. Lunney for helpful discussions; N. Carroll for technical support; and M. Padgett and P. Stamenov for lending us equipment. **Funding:** This work was supported by the Higher Education Authority of Ireland under PRTLI (Programme for Research in Third-Level Institutions) funding cycle 5 and by Science Foundation Ireland (09/SIRG/I1592, 12/RC/2278). **Author contributions:** K.E.B. performed the calculations and experiments and analyzed the data. P.R.E. devised and supervised the project. J.F.D. co-supervised the experimental work. All authors discussed the results and contributed to the writing of the manuscript. **Competing interests:** The authors declare that they have no competing interests. **Data and materials availability:** All data needed to evaluate the conclusions in the paper are present in the paper and/or the Supplementary Materials. Additional data related to this paper may be requested from P.R.E. (easthamp@tcd.ie).

Submitted 2 December 2015
Accepted 30 March 2016
Published 29 April 2016
10.1126/sciadv.1501748

Citation: K. E. Ballantine, J. F. Donegan, P. R. Eastham, There are many ways to spin a photon: Half-quantization of a total optical angular momentum. *Sci. Adv.* **2**, e1501748 (2016).

Science Advances

There are many ways to spin a photon: Half-quantization of a total optical angular momentum

Kyle E. Ballantine, John F. Donegan and Paul R. Eastham

Sci Adv **2** (4), e1501748.
DOI: 10.1126/sciadv.1501748